Enhancement of vanadium oxide doped Eu^{+3} for gas sensor application

Issam M. Ibrahim and Hassan M. Odhaib

Department of Physics, College of Science, University of Baghdad, Baghdad, Iraq

E-mail: Hassanalmoswy17@yahoo.com

Abstract

Thin films of vanadium oxide nanoparticles doped with different concentrations of europium oxide (2, 4, 6, and 8) wt % are deposited on glass and Si substrates with orientation (111) utilizing by pulsed laser deposition technique using Nd:YAG laser that has a wavelength of 1064 nm, average frequency of 6 Hz and pulse duration of 10 ns. The films were annealed in air at 300 °C for two hours, then the structural, morphological and optical properties are characterized using x-ray diffraction (XRD), Field emission scanning electron microscopy (FESEM) and UV-Vis spectroscopy respectively. The X-ray diffraction results of V_2O_5:Eu_2O_3 exhibit that the film has apolycrystalline monoclinic V_2O_5 and triclinic V_4O_7 phases. The FESEM image shows a homogeneous pattern and confirms the formation of uniform nanostructures on the glass substrate. The type of the particle found nanoparticles with different doping concentrations of Eu_2O_3. The optical energy gap increases with the increase of doping concentration and it varies from 2.67 eV to 2.71 eV. The prepared thin films are used to fabricate sensor against nitrogen dioxide gas. The dependence of sensitivity and response time on doping ratio and operation temperature of gas sensors has been studied, the maximum sensitivity was about 100%, the response time is equal to 24s and recovery time 16s for V_2O_5 doped 2% Eu_2O_3 at 50 °C.

Key words

Vanadium oxide, gas sensor, nanoparticles.

Article info.

Received: May. 2016
Accepted: Dec. 2016
Published: Jun. 2017

تحسين اوكسيد الفناديوم المشوب بمادة Eu^{+3} كمتحسس غاز

عصام محمد ابراهيم و حسن مطشر عذيب

قسم الفيزياء، كلية العلوم، جامعة بغداد، بغداد، العراق

الخلاصة

تم في هذا البحث استخدام طريقة الترسيب بالليزر النبضي بواسطة ليزر Nd:YAG ذي الطول الموجي λ=1064nm وبمعدل تكرار 6 Hz وفترة نبضة 10ns لترسيب أغشية رقيقة بنوعية عالية لاوكسيد الفناديوم النقية و المشوبه بأوكسيد اليوربيوم وبنسب مختلفة wt. % (0, 2, 4, 6, 8) على قواعد زجاجية ورقائق السليكون من النوع (111) وتم تلدين الغشاء بدرجة حرارة 300 درجة مئوية لمدة ساعتين. تم دراسة الخصائص التركيبية باستخدام حيود الاشعة السينية والمجهر الالكتروني والطوبوغرافية للسطح والخصائص البصرية باستخدام طيف الامتصاص للكيف المرئي والفق البنفسجية. بينت دراسة طيف حيود الاشعة السينية لأغشية V_2O_5 ذات التركيب النانوي وبتراكيز Eu_2O_3 مختلفة (0% - 8%) والتي تم تحضيرها باستخدام الترسيب بالليزر النبضي ان جميع الاغشيه المحضره كانت ذات تركيب متعدد التبلور وتبين أيضا ان الطور الذي ظهر في غشاء Eu_2O_3 كان أحادي الميل مع ظهور طور ثانوي و انقلاب في الطور الى V_4O_7. بينت صور المجهر الالكتروني ا شكال نانوية منتظمة الترسيب مع تغير النوع مع تغير نسبة التشويب. فجوة الطاقة البصريةتزداد بزيادة نسبة التشويب من 2.67 الى 2.71 الكترون فولت. تم استخدام الاغشية المحضرة لتصنيع متحسس لغاز اوكسيد النتروجين. تم دراسة تاثير تغيير النسبة ودرجة الحرارة على كل من التحسسية وزمن التحسس و زمن الرجوع. وجد ان اعظم تحسسية 100% وزمن تحسس 24 ثانية وزمن الرجوع 16 ثانية للعينة بنسبة 2% Eu_2O_3 وبدرجة حرارة 50 درجة مئوية.

Introduction

Controlling the free-surface electrostatic potential of semiconducting metal oxides offers possibilities for improving the performance of sensors and catalysts and photocatalysts. However, methods to exert such control have typically proven to be inexact and unreliable. The present work demonstrates an approach based on semiconductor heterojunctions, wherein an oxide substrate with controlled carrier concentration supports a much thinner layer. The layer is too thin to absorb all the charge that would normally transfer, so some of the excess charge propagates to the free surface and changes the surface potential. A combination of standard heterojunction analysis via Poisson's equation and surface potential measurements verifies the workability of this concept for thin polycrystalline V_2O_5 grown on polycrystalline anatase TiO_2 [1]. Vanadium forms various morphologies with different coordination arrangements. The most common coordination arrangements are: tetrahedral (VO_4), trigonal bipyramids or square bipyramids (VO_5) distorted and regular octahedrons (VO_6) [2, 3]. There are two bulk structures for vanadium pentoxide: α-V_2O_5 and γ-V_2O_5.The structure of α V_2O_5 has an orthorhombic layered structure. Pyramid structural arrangement builds with five oxygen atoms surrounding one vanadium atom. Vanadium forms various morphologies with different coordination arrangements [4]. Tetrahedral coordination is a preferred arrangement for +5 oxidation state [5]. The layered structure of γ-V_2O_5 resembles closely that of α-V_2O_5. As a result the γ-V_2O_5 unit cell may be obtained from that of α-V_2O_5 by a few rearrangements and twists. These twists make the γ-V_2O_5 layers more flexible but also render the structure metastable [6, 7]. The structure of vanadium pentoxide (V_2O_5) exhibits intercalation layered structure. As a result, it offers a possibility of reversible intercalations of different atoms, molecules or ions [8]. The interlayer separation of V_2O_5 changes depending the size and shape of the intercalated particles [9, 10].

Experimental

V_2O_5 nanoparticles with different doping concentrations of Eu_2O_3 (2, 4, 6, and 8) wt.% with high purity of 99.999 % is pressed under pressure of 5 ton to form a target of 1.5 cm diameter and 0.2 cm thickness. It should be as dense and homogeneous as much as possible to ensure a good quality of the deposit. Thin films of V_2O_5 with different doping ratios of Eu_2O_3 are deposited on glass and Si substrates with orientation (111) utilizing pulsed laser deposition technique the laser energy is a setup of 200 mJ with constant shoot of 600 are carried out. The distance between the targetand the substrate is 2 cm, while the distance between the target and the laser source is 12 cm. The thickness about of 100 nm, furthermore the films are annealed in air at 400 °C for two hours.

Two types of substrate were used in this study. Glass slides which were used to study the optical properties of V_2O_5: Eu_2O_3 films, and p-type Si wafer substrate with crystal orientation (111) for gas sensing measurments. Substrates cleaned using detergent with water to remove any oil or dust that might be attached to the surface of substrates, then placed under tap water and rubbing gently for 15 minutes. Then placed in a clean beaker containing distilled water, then rinsed in an ultrasonic unit for 15 minutes also.

The X-ray diffraction (XRD) pattern of the V_2O_5: Eu_2O_3 film

deposited on Si substrate is recorded by "SHIMADZU" XRD-6000 X-ray diffractmeter (CuKα radiation λ=0.154 nm), FESEM by HITACHI S4160,UV by SPECTROPHOTOMETER SP-8001.

Field emission scanning electron microscopy (FESEM) allows sample images to be quickly collected in the magnification range of 10-250,000X. In FESEM, a finely focused electron beam 5–30 keV is directed onto the examined area in a high vacuum environment. The interaction of the electron beam with the sample can yield backscattered electrons, secondary electrons, X-rays with characteristic energies, or photons. The information restored as images form or held on the area for static analysis.

Results and discussion

1. X-RAY diffraction spectra

The X-ray diffraction test is widely used as a characterization technique because it gives a lot of crystalline, lattice parameters, size of the crystallites and any other phase information about the structure of films. It is useful to determine texture and it is a non-destructive technique and requires minimum sample preparation. The interplaner distanced d_{hkl} for different planes are measured using Eq. (1)

$$n\lambda = 2d\sin\theta \quad (1)$$

Fig. 1 shows the x-ray diffraction patterns of deposit V_2O_5 thin films on Si substrates prepared by the PLD technique with different doping concentrations of Eu_2O_3 (2, 4, 6, and 8) wt. %. In pure sample there are many peaks for V_2O_5 with orientation of diffraction angle located at (12.3894°), (14.0597°), (18.7472°), (25.1582°), (27.9627°), (31.4690°), (40.7109°), (45.0390°), (50.6512°), (57.2400°), (67.3542°) identical with that of standard peaks of monoclinic structure of V_2O_5 shows in Table 1. In general there are increments in full width of half maximum with increasing doping ratio i.e. decreasing of crystalline size. There was decrease in intensities up to 4% and some peaks of V_2O_5 disappear. A new phase of vanadium oxide (V_4O_7) cubic structure was appeared at 6% and 8% with peaks ($\bar{1}20$), ($1\bar{2}2$) and (104) at diffraction angle of 26.7660°, 30.1340° and 36.2210° respectively. The increasing of doping concentrations of Eu_2O_3 lead to decrease the V_2O_5 peak intensities, as well as, the V_4O_7 peaks intensities increasing. There are no peaks appear corresponding to Eu_2O_3 in all patterns because it's low content. Sizes have been calculated depend on Scherrer's law using Eq. (2)

$$\text{Particle Size} = (0.9 \times \lambda)/(d\cos\theta) \quad (2)$$

Also it can be seen that the full width at half maximum (FWHM) increases, i.e the grain size (G.S) decrease, with increasing doping ratio. This is good result for using samples in gas sensors.

Table 1: Comparison between experimental and standard values of X-ray diffraction peaks for V_2O_5 films with different doping concentrations of Eu_2O_3.

Eu%	2θ (Deg.)	FWHM (Deg.)	d_{hkl} Exp.(Å)	G.S (nm)	hkl	d_{hkl} Std.(Å)	Phase	Card No.
Pure	12.3894	0.4167	7.1385	19.2	(100)	7.1140	V_2O_5	96-210-2584
	14.0597	1.1110	6.2940	7.2	(001)	6.2846	V_2O_5	96-210-2584
	18.7472	0.6266	4.7295	12.9	(10-1)	4.7128	V_2O_5	96-210-2584
	25.1582	0.4853	3.5369	16.8	(200)	3.5570	V_2O_5	96-210-2584
	27.9627	0.6900	3.1882	11.9	(110)	3.1920	V_2O_5	96-210-2584
	31.4690	0.6917	2.8405	11.9	(11-1)	2.8466	V_2O_5	96-210-2584
	40.7109	0.6253	2.2145	13.6	(301)	2.2178	V_2O_5	96-210-2584
	45.0390	0.5538	2.0112	15.5	(-103)	2.0089	V_2O_5	96-210-2584
	50.6512	0.7615	1.8008	11.5	(020)	1.6117	V_2O_5	96-210-2584
	57.2400	1.1106	1.6081	8.2	(-213)	1.6117	V_2O_5	96-210-2584
	67.3542	0.4853	1.3892	19.7	(321)	1.3910	V_2O_5	96-210-2584
	70.5186	0.6934	1.3344	14.0	(-123)	1.3351	V_2O_5	96-210-2584
2%	12.4068	0.5634	7.1286	14.2	(100)	7.114	V_2O_5	96-210-2584
	18.7735	0.8472	4.7229	9.5	(10-1)	4.7128	V_2O_5	96-210-2584
	25.1934	0.6561	3.5321	12.4	(200)	3.557	V_2O_5	96-210-2584
	28.0019	0.7650	3.1839	10.7	(110)	3.192	V_2O_5	96-210-2584
	31.5131	0.7340	2.8367	11.3	(11-1)	2.8466	V_2O_5	96-210-2584
	40.7679	0.8454	2.2115	10.0	(301)	2.2178	V_2O_5	96-210-2584
	45.1020	0.7488	2.0086	11.5	(-103)	2.0089	V_2O_5	96-210-2584
	57.3202	1.5015	1.6061	6.0	(-213)	1.6117	V_2O_5	96-210-2584
	67.4485	0.6561	1.3874	14.6	(321)	1.391	V_2O_5	96-210-2584
	70.6173	0.9375	1.3327	10.4	(-123)	1.3351	V_2O_5	96-210-2584
4%	12.4241	0.7618	7.1186	10.5	(100)	7.114	V_2O_5	96-210-2584
	18.7997	1.1454	4.7164	7.0	(10-1)	4.7128	V_2O_5	96-210-2584
	25.2287	0.8870	3.5272	9.2	(200)	3.5570	V_2O_5	96-210-2584
	28.0411	0.8000	3.1795	10.2	(110)	3.1920	V_2O_5	96-210-2584
	31.5572	0.9700	2.8328	8.5	(11-1)	2.8466	V_2O_5	96-210-2584
	40.8250	1.1430	2.2086	7.4	(301)	2.2178	V_2O_5	96-210-2584
6%	26.7660	0.7557	3.3280	10.8	(-120)	3.3271	V_4O_7	96-100-8026
	28.0073	0.5104	3.1833	16.1	(110)	3.1920	V_2O_5	96-210-2584
	30.1560	0.4096	2.9612	20.1	(1-22)	2.9701	V_4O_7	96-100-8026
	36.2100	0.5633	2.4788	14.8	(104)	2.478	V_4O_7	96-100-8026
	40.6540	0.4625	2.2175	18.3	(301)	2.2178	V_2O_5	96-210-2584
	44.9760	0.4096	2.0139	21.0	(-103)	2.0089	V_2O_5	96-210-2584
	51.1900	0.8215	1.7831	10.7	(020)	1.6117	V_2O_5	96-210-2584
8%	26.7660	0.7587	3.3280	10.8	(-120)	3.3271	V_4O_7	96-100-8026
	28.0080	0.5173	3.1832	15.8	(110)	3.192	V_2O_5	96-210-2584
	30.1340	0.6196	2.9633	13.3	(1-22)	2.9701	V_4O_7	96-100-8026
	36.2210	0.5633	2.4780	14.8	(104)	2.478	V_4O_7	96-100-8026
	44.9550	0.4076	2.0148	21.1	(-103)	2.0089	V_2O_5	96-210-2584
	51.1876	0.8233	1.7832	10.7	(020)	1.6117	V_2O_5	96-210-2584

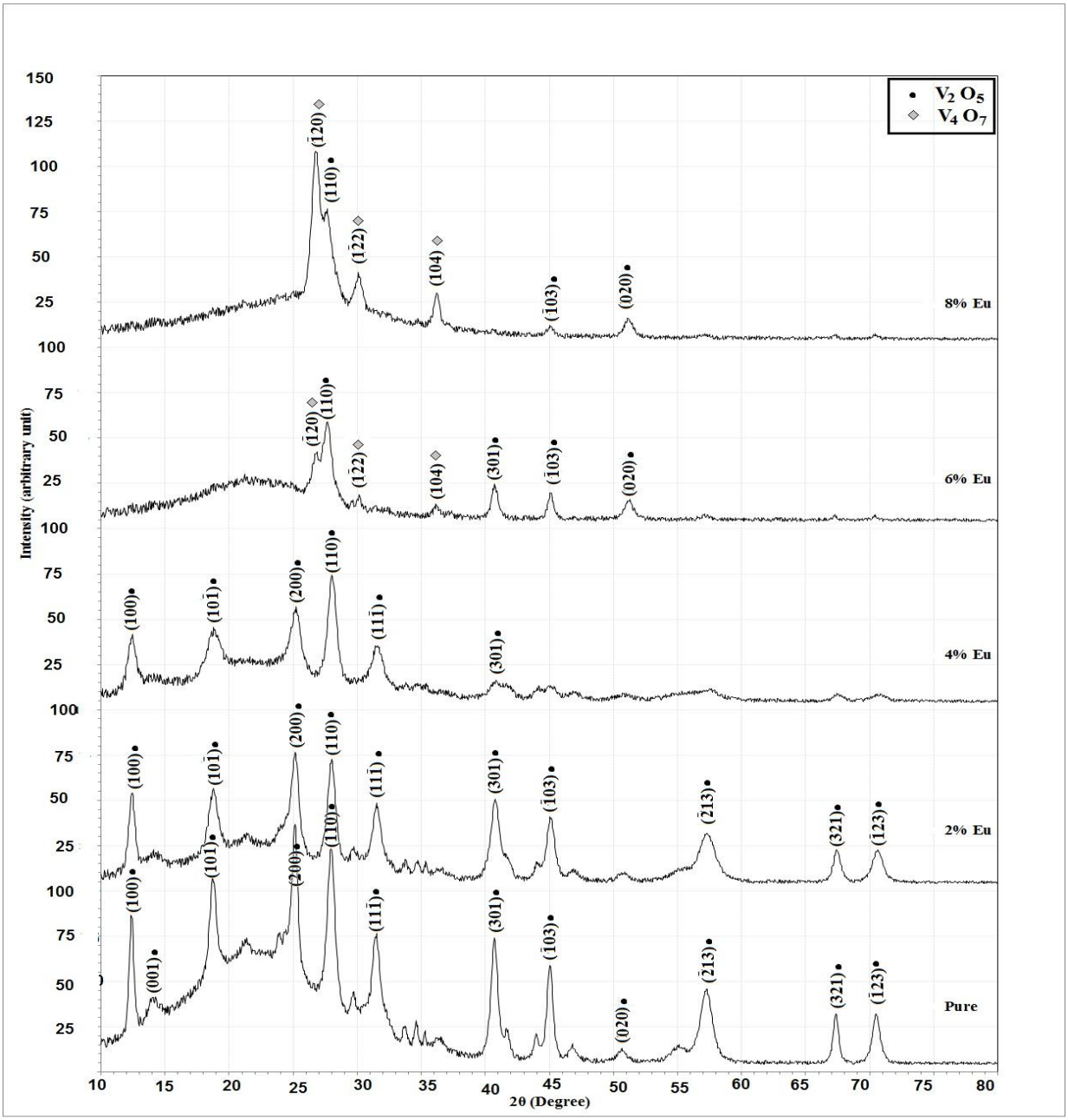

Fig.1: XRD for V_2O_5: Eu_2o_3 at annealing temperature of 300 °C.

2. Field emission scanning electron microscope (FESEM)

Field emission scanning electron microscope (FESEM) can be used to obtain three dimensions like topographical images of a wide variety of samples. FESEM images of undoped and doped films with different concentration of Eu_2O_3 were shown in Fig. 2. The FESEM image shows a homogeneous pattern and confirms the formation of uniform structures on the glass. The size of the particles of pure and doped with 2%, 4%, 6%, 8% wt of Eu_2O_3 are in the range of nanostructure. The Nano particle size decrease from 200 nm in pure samples to less than 50 nm at 8% sample.

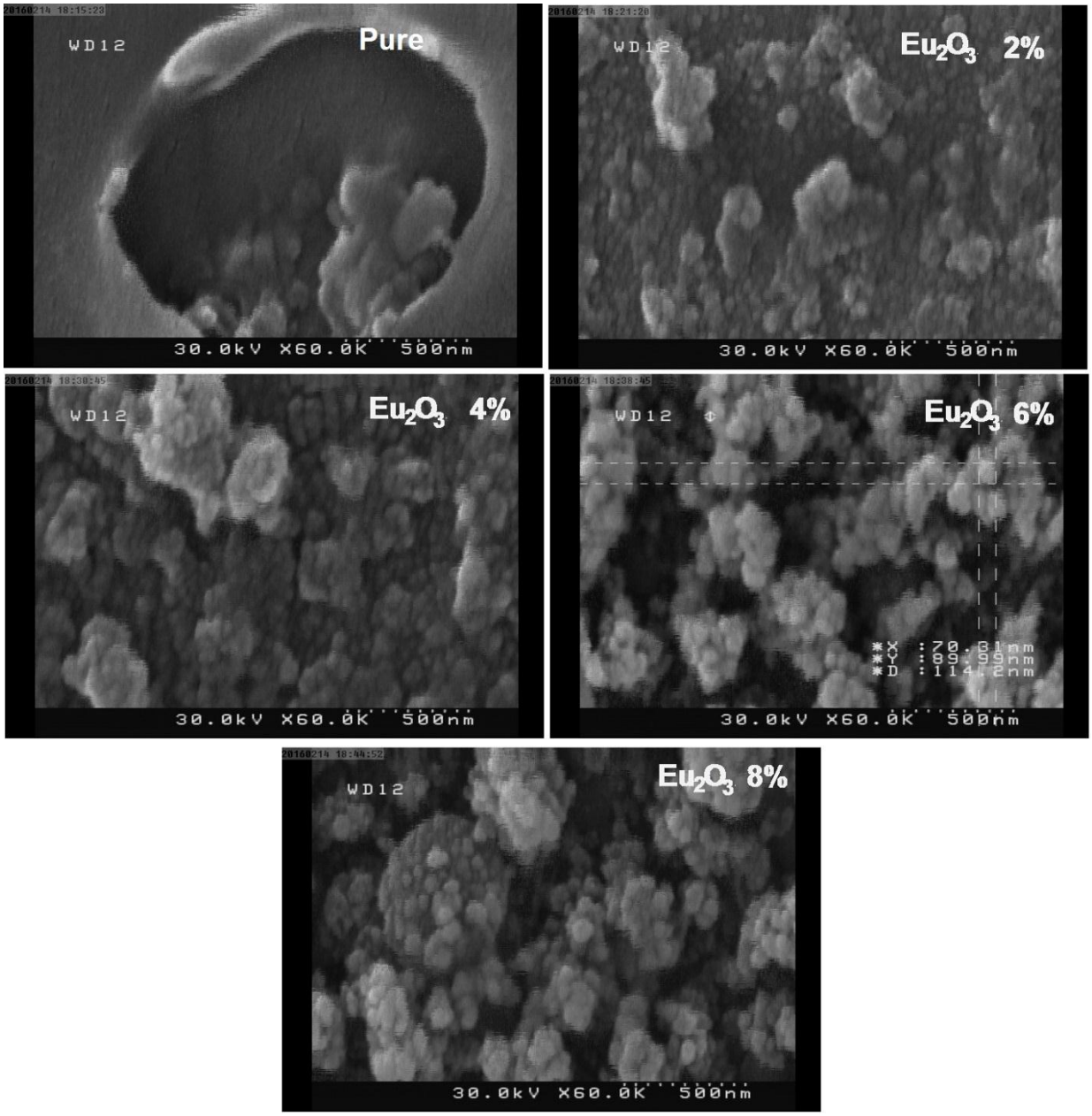

Fig.2: FESEM for V_2O_5:Eu_2O_3 at room temperature.

3. Optical Properties

Fig.3 shows the transmittance of V_2O_5 doped with different concentration of Eu_2O_3. There was increasing in transmittance accompanied increase of Eu_2O_3 doping rate. There was stability in transmittance about 90% from 500 nm to 1100 nm. Spectrum is a significantly associated with the structure of energy levels which are in turn connected with chemical and crystalline structure of the material and therefore general characteristics of that material. Fig. 3 shows the variation of transmittance for deposited V_2O_5 thin films on glass substrates with wavelength for different doping ratio with E_2O_3. It clear from this figure that the transmission for all films about 90% at the range 500 to 1100 nm and increase with increasing doping ratio, which is useful for used as optically transparent films.

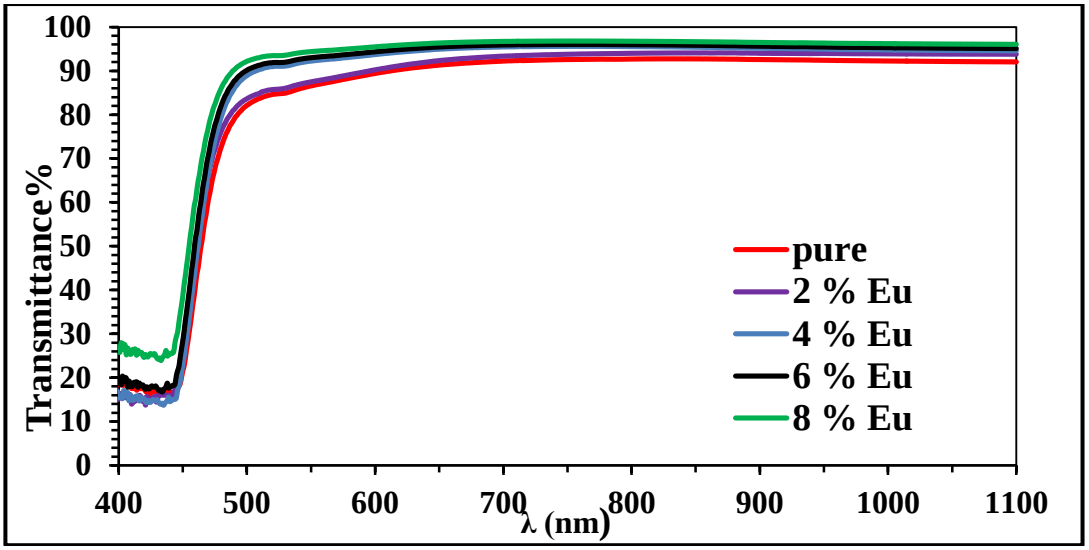

Fig.3: Transmittance as a function of wavelength for V_2O_5 films doped with (2, 4, 6, and 8)wt %. Eu_2O_3.

Fig. 4 shows the variation of absorption coefficient (α) for V_2O_5 film with wavelength at different doping of Eu_2O_3 (2, 4, 6 and 8) wt. %. The absorption coefficient has opposite behavior as compared to the transmittance. It can be seen that the absorption edge is shifted to less values of wavelength with increasing of doping concentration. Absorption is expressed in terms of a coefficient (α), which is defined as the relative rate of decrease in light intensity along its propagation path, and the main reason for this attenuation is attributed to the absorption processes. The measurement of absorption coefficient, particularly near the fundamental absorption edge, provides a standard method for the investigation of optically induced electronic transitions and gives some idea about the band structure and energy gaps in both pure and doped V_2O_5.

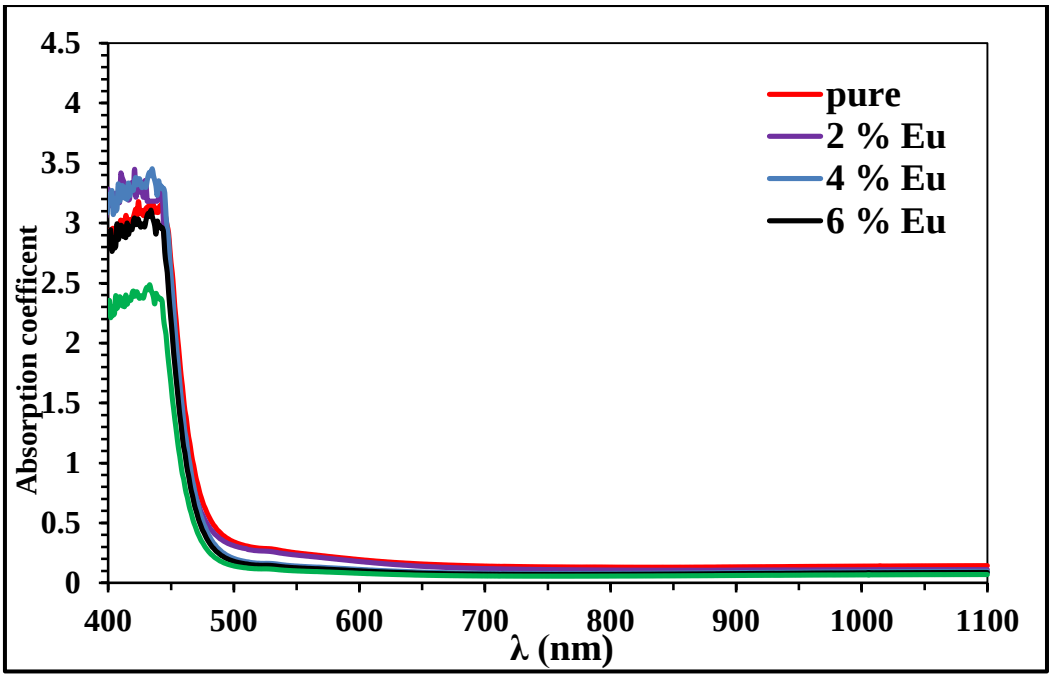

Fig.4: Absorption coefficient as a function of wavelength for V_2O_5 films doped with (2, 4, 6, and 8) wt %. Eu_2O_3 ratio.

The values of optical energy gap and the type of the optical transition for V_2O_5 films with different doping concentrations of Eu_2O_3 deposited on glass substrate at R.T. The optical energy gap (Eg^{opt}) have been determined using Tauc equation by the extrapolation of the portion at $(\alpha h\upsilon)^2$ =0 in Eq.(3). The energy gap increases with increase of doping concentration and it was variation from 2.670 eV to 2.710 eV show in Fig. 5. It can be observed that (Eg^{opt}) increases slightly and shifting towards the ultra-violate region as the concentration increases of Eu_2O_3 this is because of the effect of impurity or disorder and some defects in semiconductors leads to local electric fields that affect the band tails near the band edge. Also the size effect for nanostructure makes this shift. The results of optical energy gap indicate that all the films have localized states which result from the density of defects at the grain boundaries and donor levels, so we can conclude that the optical energy gap can be controlled through the control of impurities ratios and the size of nanostructure. Best fit line intersects the energy photon axis at (hυ) equal to zero which represents the values of optical energy gap

$$\alpha\,(h\nu)=B\,(h\nu-Eg^{opt})^{r} \qquad (3)$$

where: h: is the plank constant. α: is the absorption coefficient. hν: is the incident energy. r: is constant which takes the values (1/2, 3/2, 2, 3) depending on the material and the type of the optical transition whether it is direct or indirect. Eg^{opt}: is optical energy gap, where B is a constant inversely proportional to amorphousity.

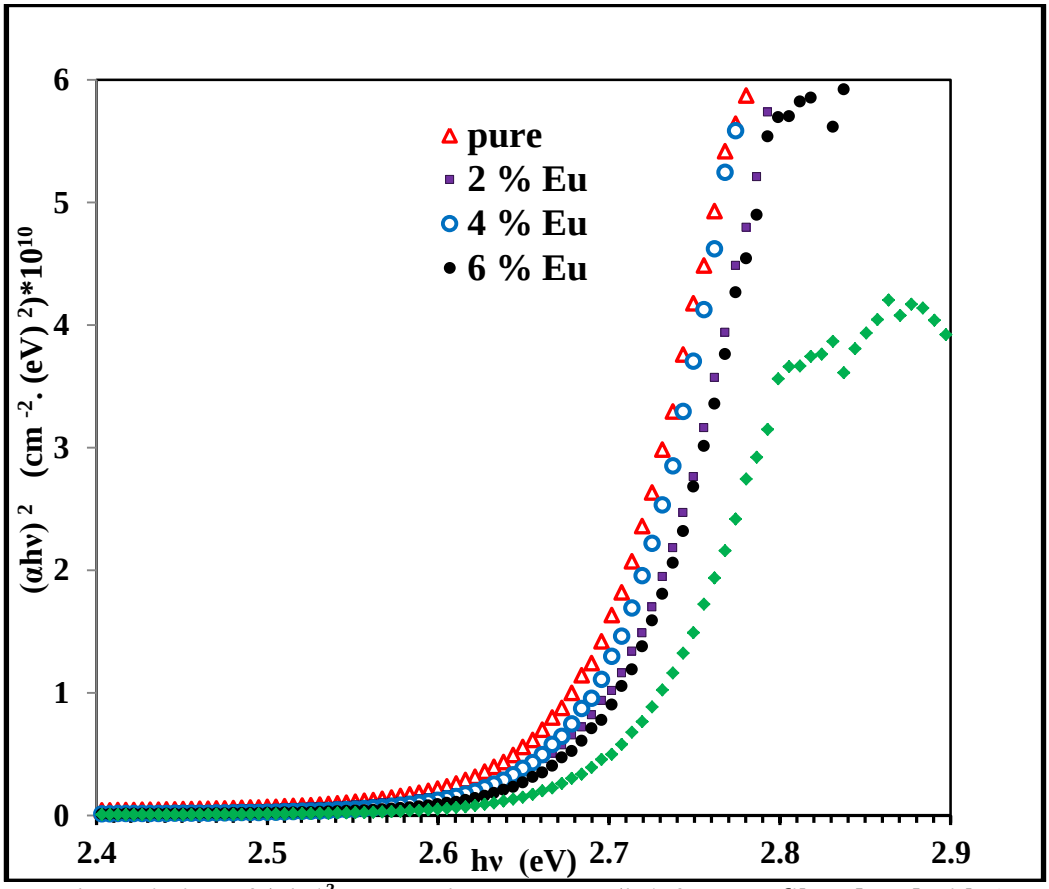

Fig.5: The variation of $(\alpha h\upsilon)^2$ versus photon energy (hυ) for V_2O_5 films doped with (2, 4, 6, and 8) wt %. Eu_2O_3 ratio.

4. Gas sensor measurements

Fig. 6 shows the variation of resistance as a function of the time with on/off gas valve. The resistance of gas sensor decreases exponentially when open the gas till reach the minimum value and the action reverse with gas closing, because it is p-type. Gas sensor measurement of pure and doped V_2O_5 show high sensitivity to NO_2 gas, and the sensitivity was increases with the increase of operation temperature. The maximum sensitivity was found about 100% and the best response time is equal to 24s, while, recovery time 16s for 2% Eu_2O_3 sample at 50 °C. All gas sensors parameters were shown in Table 2.

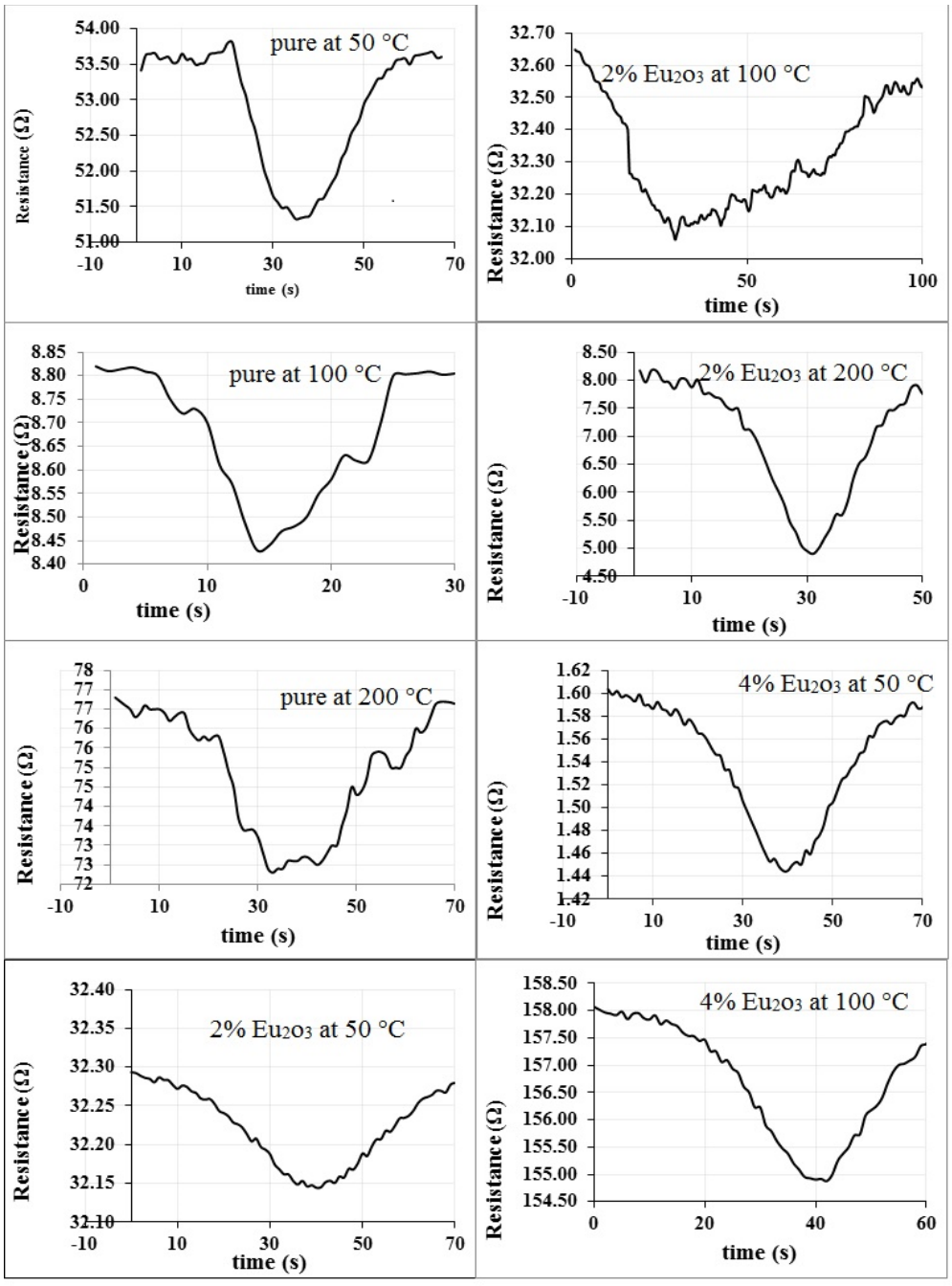

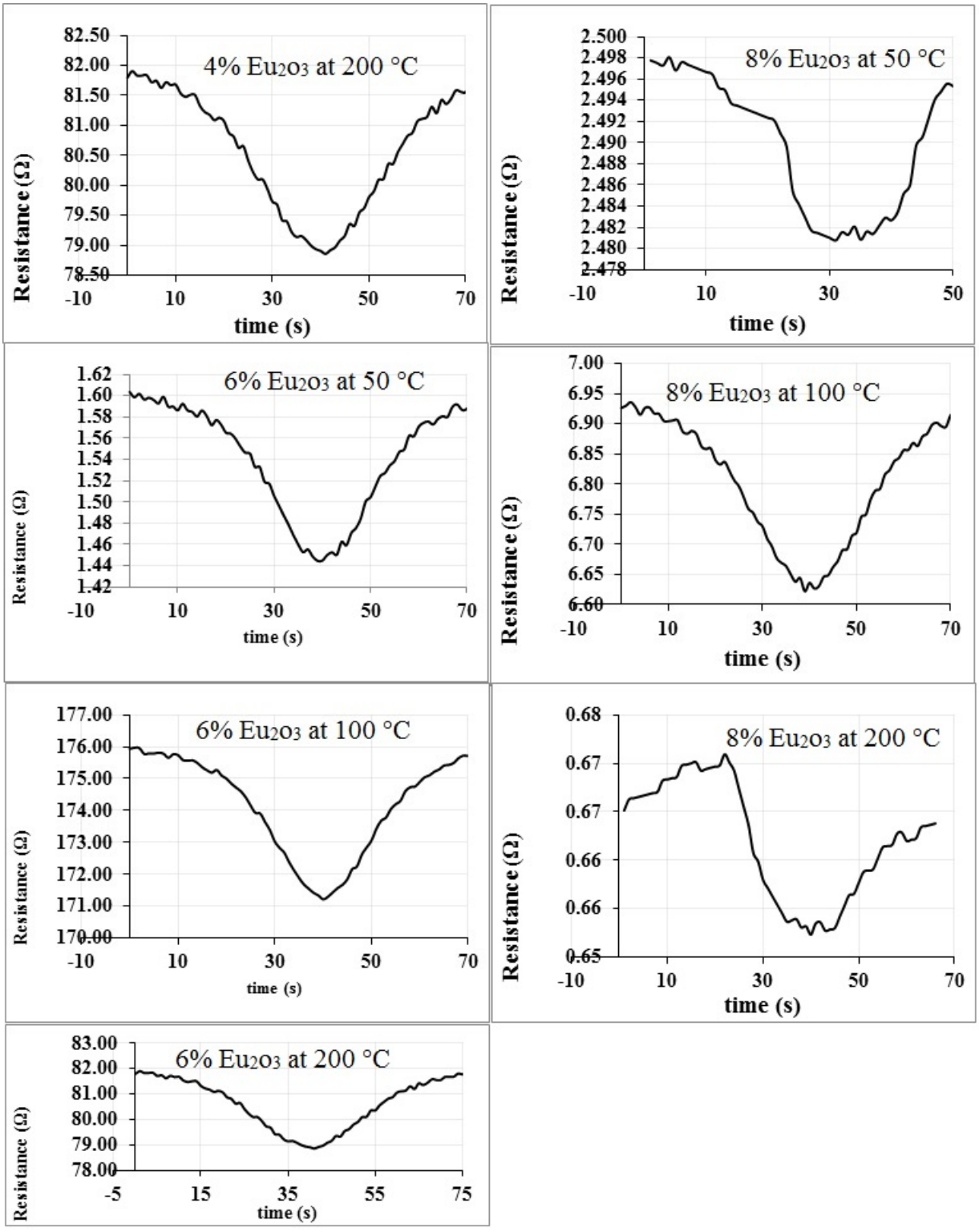

Fig.6: The variation of resistance as a function to the time for V_2O_5 films doped with (2, 4, 6, and 8) wt %. Eu_2O_3 ratio.

Table 2: The sensitivity, response and recovery time.

PURE	Sensitivity%			Response time (sec)			Recovery time (sec)		
	50°C	100°C	200°C	50°C	100°C	200°C	50°C	100°C	200°C
	96	96	95	18	8	21	27	7	23
2%	100	98	60	24	28	19	16	53	18
4%	90	97	96	24	33	30	28	26	31
6%	90	98	96	24	27	27	26	29	28
8%	99	95	97	24	28	18	14	27	18

Conclusions

Polycrystalline V_2O_5-doped Eu_2O_3 structures were successfully prepared by PLD technique. The x-ray diffraction reveals that there was decrease in intensities up to 4% and some peaks of V_2O_5 disappear. A new phase of vanadium oxide (V_4O_7) cubic structure was appeared at 6% and 8% with peaks ($\bar{1}20$), ($1\bar{2}2$) and (104) at diffraction angle of 26.7660°, 30.1340° and 36.2210° respectively. The FESEM image shows a homogeneous pattern and confirms the formation of uniform structures on the glass. The maximum sensitivity is 100% and the best response time is equal to 24s, while, recovery time 16s for 2% Eu_2O_3 sample at 50 °C.

References

[1] K. Navaneetha. Nandakumar, Edmund G. Seebauer, J. Phys. Chem. C, 120, 10 (2016) 5486–5494.

[2] C. Ban, "Synthesis and Characterization of nano scale Vanadium Oxides, Vanadium Phosphates as Cathodes for Lithium Batteries", New York: UMI Dissertations Publishing, p.195, 2008.

[3] P. Tsolov, "Design fabrication and characterization of thick-film gas sensors," Rovira Univ., 2004.

[4] E. Londero, E. Schroder, Physical Review B, 82, 5 (2010) 8-10.

[5] G. Andersson, Acta Chemica Scandinavica, 8, 9 (1954) 1599-1606.

[6] R. Levi, M. Bar-Sadan, A. Albu-Yaron, R. Popovitz-Biro, L. Houben, Y. Prior, R.Tenne, Materials (Basel)., 3, 8 (2010) 4428–4445.

[7] G. Cao and R. Pacific Northwest National Laboratory (PNNL) WA (US), Environmental Molecular Sciences Laboratory (EMSL), J. Am. Chem. Soc., 18, 12 (2006) 2787-2804.

[8] V. Zepf, "Rare Earth Elements: What and Where They Are," in Rare Earth Elements, Chapter 2, Springer Link, (2013) 11–39.

[9] V. Grasso, "Rare Earth Elements in National Defense: Background, Oversight Issues, and Options for Congress," p. 43, 2013.

[10] J. Parker, U. Geiser, D.Lam, Y.W. Y. Ching, Journal of the American Ceramic Society, 73, 11 (1990) 3206-3208.